Titel Page:

Novel Conformation Specific Inhibitors of Activated GTPases reveal Ras-dependency of Patient-Derived Cancer Organoids

Authors:

Svenja Wiechmann[1,2], Pierre Maisonneuve[3], Britta M. Grebbin[4,5,6], Meike Hoffmeister[1,7], Manuel Kaulich[1,8], Hans Clevers[9,10,11], Krishnaraj Rajalingam[12], Igor Kurinov[13], Henner F. Farin[4,5,6], Frank Sicheri[3] and Andreas Ernst[1,2,*]

Affiliations:

[1]Institute of Biochemistry II, Goethe University Frankfurt - Medical Faculty, University Hospital, Frankfurt am Main, Germany.

[2]Fraunhofer Institute for Molecular Biology and Applied Ecology IME, Project Group Translational Medicine and Pharmacology TMP, Theodor-Stern-Kai 7, 60590 Frankfurt am Main, Germany.

[3]Lunenfeld-Tanenbaum Research Institute, Sinai Health System, Toronto, ON M5G 1X5, Canada.

[4]German Cancer Consortium (DKTK), 69120 Heidelberg, Germany.

[5]Georg-Speyer-Haus, Institute for Tumor Biology and Experimental Therapy, 60596 Frankfurt am Main, Germany.

[6]German Cancer Research Center (DKFZ), 69120 Heidelberg, Germany.

[7]Institute of Biochemistry, Brandenburg Medical School (MHB) Theodor Fontane, Neuruppin and Brandenburg an der Havel, Germany.

[8]Frankfurt Cancer Institute, Frankfurt am Main, Germany.

[9]Hubrecht Institute, Royal Netherlands Academy of Arts and Sciences (KNAW) and University Medical Center (UMC) Utrecht, Netherlands.

[10]Cancer Genomics Netherlands, UMC Utrecht, Netherlands.

[11]Center for Molecular Medicine, Department of Genetics, UMC Utrecht, Netherlands.

[12]Molecular Signaling Unit-FZI, Institute of Immunology, University Medical Center Mainz, JGU-Mainz, Germany.

[13]Department of Chemistry and Chemical Biology, Cornell University, NE-CAT, Argonne, IL 60439, USA.

[*]Corresponding author: Andreas Ernst (a.ernst@em.uni-frankfurt.de)

Abstract:

The small GTPases H, K, and NRAS are molecular switches that are indispensable for proper regulation of cellular proliferation and growth. Mutations in this family of proteins are associated with cancer and result in aberrant activation of signaling processes caused by a deregulated recruitment of downstream effector proteins. In this study, we engineered novel variants of the Ras-binding domain (RBD) of the kinase CRAF. These variants bound with high affinity to the effector binding site of active Ras. Structural characterization showed how the newly identified mutations cooperate to enhance affinity to the effector binding site compared to RBDwt. The engineered RBD variants closely mimic the interaction mode of naturally occurring Ras effectors and as dominant negative affinity reagent block their activation. Experiments with cancer cells showed that expression of these RBD variants inhibits Ras signaling leading to a reduced growth and inductions of apoptosis. Using the optimized RBD variants, we stratified patient-derived colorectal cancer organoids according to Ras dependency, which showed that the presence of Ras mutations was insufficient to predict sensitivity to Ras inhibition.

51 **Main Text:**

52 **Introduction**

53 The small GTPases H, K, and NRAS are molecular switches that relay signals from growth
54 factor receptor tyrosine kinases to transcription factors and other intracellular mediators to
55 affect the growth, proliferation, and survival of cells. To achieve this function, the
56 conformation of Ras GTPases cycles between an inactive, guanosine 5'-diphosphate (GDP)-
57 bound state and an active, guanosine 5'-triphosphate (GTP)-bound state that interacts with
58 downstream effector proteins. Along this reaction cycle, the weak hydrolysis activity of Ras
59 is enhanced by GTPase activating proteins (GAPs), and guanine exchange factors (GEFs)
60 facilitate the discharge of GDP and the reloading with GTP. In cancer, mutations in members
61 of the Ras family shift the fine-tuned equilibrium of this reaction cycle toward the active,
62 GTP-bound state, resulting in constitutive activation of downstream kinases. The resulting
63 uncoupling of the regulatory link between proliferation and upstream receptor signaling
64 leads to uncontrolled growth and proliferation. Thus, mutated Ras GTPases are oncogenic
65 drivers in various malignancies making them, and their downstream effector kinases, a
66 major focus for the development of anti-proliferative drugs.

67 When in active conformation, Ras GTPases propagate signals by the recruitment of
68 kinases of the Raf family, thereby stimulating growth factor signaling pathways[1]. Members
69 of this family of kinases interact with several different GTPases of the Ras subfamily. For
70 example, BRAF is activated by oncogenic Ras and by the GTPase Rap1 [2, 3]. In a two-hybrid
71 assay, the kinases ARAF and CRAF interact with the closely Ras-related GTPase RRAS [4].
72 Furthermore, the CRAF Ras binding domain (RBD) crystallized in complex with either HRAS or
73 RAP1A, indicating that both interactions are sufficiently strong to yield co-crystal structures
74 [5, 6]. This multi-specificity of Raf kinases relates to the conservation of the effector binding
75 site and RBD at the atomic molecular level[7]. Thus, reagents that interfere with the Ras/Raf
76 interaction are likely to efficiently inhibit the activation of growth signals over a wide range
77 of conditions.

78 Developing inhibitors of Ras has been challenging because of the high affinity of
79 guanosine di/tri-phosphate (GDP/GTP) for the GTP binding pocket of the Ras family of
80 proteins and due to the flat topology of the conserved effector binding site [8, 9].
81 Consequently, to date, only a few small molecule inhibitors exist that directly interfere with
82 Ras function [10]. To overcome the paucity of small molecules that directly interfere with

83 Ras activity, several affinity reagents based on protein scaffolds have been developed to
84 address different facets of Ras biology. For example, fibronectin-derived monobodies inhibit
85 signaling by disrupting the dimerization of H and KRAS at the plasma membrane [11].
86 Interfering with Ras dimerization limits the growth of xenografts that inducibly express the
87 monobody [12]. An alternative strategy for inhibiting Ras signaling with engineered proteins
88 is to prevent the recruitment of downstream effectors or block the activation of Ras by GEFs.
89 To this end, affinity reagents have been generated that compete with Ras effectors by
90 selectively binding to the active or inactive state of oncogenic Ras [13-19]. However, several
91 required high concentrations to be effective in cells [16, 17, 20], and their selectivity for
92 members of the Ras family is unknown. The limited effectiveness may be related to the
93 interaction of Raf family kinases with various Ras GPTases. Thus, a rationale for affinity
94 reagents with improved efficacy could be those that block interactions with multiple Ras
95 family members simultaneously.
96 An ideal affinity reagent that inhibits Ras function should avoid steric constraints by
97 precisely replicating effector binding to activated, GTP-bound Ras. Additionally, these affinity
98 reagents should have a high affinity to the effector binding site and the ability to
99 outcompete downstream effectors. Consequently, such an affinity reagent would act as
100 inhibitor of Ras signaling, which could be used to probe the biology of Ras inhibition in
101 cellular and patient-derived model systems. To derive an affinity reagent that fulfills these
102 criteria, we adapted our strategy of optimizing pre-existing intermolecular contacts [21, 22]
103 to the RBD of CRAF. We constructed a phage-displayed RBD library encoding mutations of
104 interface residues and selected for improved binding to active, GTP-bound Ras. Crystal
105 structures of complexes with activated HRAS G12V showed that the RBD variants (RBDvs)
106 precisely mimic effector binding, and the engineered mutations subtly improve
107 intermolecular contacts. Importantly, intracellular expression of individual RBDvs resulted in
108 impaired growth of various cancer cell lines due to a robust inhibition of Ras signaling and
109 the MAP kinase signaling cascade. Finally, in patient-derived organoids, the differential
110 effects of the RBDvs on cellular growth and metabolic activity revealed differences in Ras
111 dependency of colorectal tumor organoids, demonstrating that genetic data were
112 insufficient to predict responsiveness to Ras inhibition. The ability of the RBDvs to inhibit
113 growth of cells lacking activating mutations in Ras family members may relate to their

114 multispecificity in interacting with active conformations of Ras GTPases with a conserved
115 switch 1 region.
116
117 **Results**
118 **Engineered RBD variants have high affinity for GTP-bound Ras and compete with effector**
119 **binding *in vitro***
120 Previous studies demonstrated that the CRAF-RBD is highly tolerant to mutations and can be
121 computationally engineered to preferentially bind inactive states of Ras [18, 23, 24]. To
122 optimize the interface of the RBD to active Ras, we analyzed existing crystal structures of
123 Ras:RBD complexes [5, 25, 26]. In total, we identified 14 residues that make sidechain
124 contacts to the switch-1 region of the Ras effector binding site. These residues are located
125 on the β1-β2 hairpin and α1 helix, and span two distinct regions of the CRAF-RBD. To
126 achieve a moderate to low mutation rate that does not alter the binding mode nor impair
127 the structure of the RBD, we used a soft randomization strategy that allowed 70% of the
128 wild-type nucleotides and 10% of the non-wild-type nucleotides to occur at any codon
129 position encoding the targeted residues (**Fig. 1A**). Additionally, we replaced three unpaired
130 cysteines at position 81, 95, and 96 of the RBD with serine residues to prevent dimerization
131 of phage-displayed proteins and improve overall presentation of the RBDvs. Our final library
132 contained more than $2x10^9$ unique RBDvs presented on the surface of filamentous phage
133 and subsequent selection by phage display yielded 5 variants with improved binding to
134 surface immobilized GTPγS-loaded HRAS (**Fig. 1B**). The selected variants show a conserved
135 mutational pattern, indicating a shared binding mode to activated Ras. Strikingly, the
136 mutation Gln^{66} to Glu is highly enriched in all 5 variants, indicating that this mutation has a
137 crucial role in mediating the increased affinity. Coincidentally, the mutation from Val^{88} to
138 Arg, previously shown to increase the affinity of RBD to HRAS [27], was also present in all 5
139 variants. An Arg^{89} to His mutation occurred in four of the five RBDvs.
140 After purification as His-tagged proteins, we tested if the engineered RBDvs
141 outcompeted CRAF-RBDwt binding to GTPγS-loaded KRAS *in vitro* (**Fig. 1C**). Relative to
142 RBDwt, all engineered variants showed an enhanced ability to compete off GTPγS KRAS in
143 solution. A similarly enhanced competitive ability of the RBDvs was observed using the Ras
144 association domain (RA) of Ral Guanine Nucleotide Dissociation Stimulator (RalGDS) instead

145 of the CRAF-RBDwt (**Supplementary Fig. 1A**). Because RBDv1 and RBDv12 performed best in
146 these experiments, we focused our further analysis on these two variants.
147 Affinity measurements confirmed that RBDv1 and RBDv12 have improved binding
148 properties relative to RBDwt for activated HRAS with K_ds of ~ 3 nM versus ~60 nM and
149 strongly preferred binding to activated, GTPγS loaded HRAS with negligible binding to the
150 GDP-bound form (**Fig. 1D)**. In control experiments, we confirmed that His-tagged HRAS
151 GTPγS does not bind to GST-loaded sensors or empty sensors alone (**Supplementary Fig. 1B**),
152 indicating that the slow off rate is not due to non-specific binding of HRAS to GST or the
153 sensor material.
154
155 **The engineered RBDvs mimic effector binding to active Ras**
156 To understand the structural basis for improved binding, we crystallized HRAS G12V in
157 complex with RBDv1 at 2.9 Å and RBDv12 at 3.15 Å resolution in an active conformation (**Fig.**
158 **2A, Supplementary Table 1**). Structural analysis revealed that the RBDvs engaged the
159 effector binding site of HRAS through a canonical binding mode [5] with only minor shifts to
160 the center of mass positions and rotation angle (1.8 Å/15˚ and 2.0 Å/16˚ for RBDv1 and
161 RBDv12, respectively). Similar to the canonical binding mode of RBDwt, β2 of the RBDvs
162 forms an extended intermolecular β-sheet with β2 of HRAS (**Supplementary Fig. 2A**). In
163 addition, helices α1 of both RBDwt and RBDvs form direct contacts with switch 1 residues in
164 Ras (**Fig. 2A**). Inspection of direct contact interface reveals that the conserved RBDvs
165 mutations of Gln^{66} to Glu, Val^{88} to Arg, and Arg^{89} to His result in a rewiring of the hydrogen
166 (H)-bonding pattern to the Asp^{38} and Tyr^{40} side chains in HRAS (**Fig. 2B**). This change in H-
167 bonding pattern together with steric effects involving Ile^{21} in HRAS and Val^{88} to Arg in RBDvs
168 appears responsible for a shift of the α1-helix of the RBDvs relative to that observed in
169 RBDwt (**Fig. 2C**). In summary, our combinatorial approach to RBD-interface engineering
170 identified three key mutations that work together to improve contacts to residues in the
171 switch 1 region of Ras in an active conformation. Because the binding mode of RBDvs to
172 HRAS overlaps completely with RBDwt, the RBDvs are expected to outcompete binding of
173 Ras effectors that engage this common binding site.
174
175 **The RBDvs bind Ras GTPases in cells**

176 We tested the intracellular specificity of the RBD variants using mass spectrometry. We
177 immunoprecipitated hemagglutinin (HA)-tagged RBDvs and HA-RBDwt that were inducibly
178 expressed in stably transduced colon carcinoma HCT 116 cells (**Supplementary Fig. 3A and**
179 **B**). HCT 116 are heterozygous for the activating mutant KRAS G13D. Strikingly, relative to
180 RBDwt, RBDv1 and RBDv12 displayed up to 5500-fold enrichment of peptides from
181 endogenous KRAS4B G13D isoform (**Fig. 3A, Supplementary Table 2)**. The prevalence of
182 peptides originating from the constitutively active KRAS4B G13D isoform suggests that the
183 RBDvs preferentially interact with Ras GTPases, which are in an active conformation.
184 We also detected peptides from other Ras family GTPases, although these were ~10-
185 fold less abundant than KRAS4B G13D peptides. Analysis of the primary sequences of the
186 other Ras family members that interacted with the RBDvs showed that these Ras family
187 members share a common effector binding site (**Fig. 3B**). In particular, the detected peptides
188 were from Ras family members containing D^{38} and Y^{40} residues in their respective switch-1
189 region, which we identified as key interaction residues for the RBDvs (**Fig. 2B**). Thus, the
190 immunoprecipitation data showed that RBDvs bind to their intended targets, Ras proteins, in
191 cells, and exhibit the highest affinity for active Ras.
192 Consequently, these results suggested that the RBDvs are dominant-negative affinity
193 reagents that will not only impair signaling through constitutive active Ras mutants but also
194 other Ras GTPases in the active conformation. Thus, the RBDvs have the potential to inhibit
195 multiple Ras-mediated pathways to Raf activation. Furthermore, the simultaneous inhibition
196 of multiple Ras GTPases is potentially an efficient way to control the proliferation of cells
197 with heterozygous KRAS genotypes, which confer resistance to MEK inhibitors [28].
198
199 **RBDvs inhibit activation of the ERK and AKT pathways resulting in reduced metabolic**
200 **activity and apoptosis**
201 To test if the RBDvs act as inhibitors of Ras-dependent signaling processes, we probed whole
202 cell lysates from cell lines expressing HA-tagged RBDvs or RBDwt with antibodies detecting
203 the phosphorylation state of kinases downstream of Ras proteins. Specifically, we examined
204 the effect of inhibition of Ras/Raf interaction in cell lines of different cancer origins and with
205 different Ras mutations (**Supplementary Table 3**). Immunoblot analysis showed that the
206 RBDvs reduced the phosphorylation of the growth signal-activated ERK1/2 in HCT 116, Mia
207 PaCa-2, A549, and H1299 cells (**Fig. 4A**). The corresponding control experiments with RBDwt,

208 despite its higher expression, did not reduce ERK1/2 phosphorylation, indicating that the
209 improved affinity of the RBDvs for active Ras isoforms is required to suppress activation of
210 these downstream kinases.
211 Reduced activity of MAP kinase pathway often results in reduced cell viability.
212 Therefore, we measured ATP content, as an indicator of metabolic activity and viability, and
213 monitored growth curves, as an indicator of proliferation. In all 4 cell lines, inhibition of
214 effector binding to active Ras by the RBDvs reduced cell viability (ATP content) (**Fig. 4B**),
215 indicating that the RBDvs disrupt Ras signaling in cells from different cancer backgrounds.
216 Importantly, RBDwt control had only minimal effects on the viability of all 4 cell lines. Five-
217 day growth curves measured with HCT116 cells confirmed that the RBDvs, but not RBDwt,
218 inhibited proliferation (**Fig. 4C**).
219 Ras signaling not only mediates proliferative responses, but these GTPases also
220 promote cell survival. In the presence of the RBDvs, HCT 116 cells exhibited reduced
221 phosphorylation of Ser^{473} in the serine/threonine kinase AKT, indicating that PI3 kinase
222 pathway is inhibited (**Fig. 4D**). Together, the reduced MAP kinase and PI3 kinase pathway
223 activity could not only reduce cellular metabolic activity and proliferation but could also
224 increase apoptosis. We monitored HCT116 cells expressing either RDBvs or RBDwt for
225 annexin V staining as an indicator of apoptotic cells (**Fig. 4E, Supplementary Fig. 4**).
226 Quantification of annexin V staining by flow cytometry revealed that HCT116 cells expressing
227 the RBDvs had significantly increased number of apoptotic cells compared to non-induced
228 controls and compared to induced cells expressing RBDwt. In summary, these results
229 showed that the RBDvs inhibit the ERK and PI3K signaling pathway, resulting in growth
230 reduction in a wide range of cancer cell lines and inducing apoptosis in HCT116 cells.
231
232 **RBDvs lead to reduced growth in patient-derived colorectal cancer organoids**
233 To investigate whether the characteristics of our RBDvs in cell culture can be translated into
234 a patient-derived model, we used tumor organoids with known Ras mutation status isolated
235 from surgically removed colorectal carcinoma from 7 patients [29] (**Table 1**). After
236 transduction with the doxycycline-inducible lentiviral constructs, we compared cell viability
237 and growth of organoids, cultured in Matrigel and expressing RBDvs or RBDwt. We
238 evaluated by immunoblot of organoid lysates ERK and AKT phosphorylation in response to
239 doxycycline-induced expression of the RBDvs or RBDwt (**Fig. 5A, Supplementary Figure 5A**).

240 The different organoids showed different sensitivity to the inhibitory effects of the RBDvs on
241 these two kinases. For example, P17T with wild-type KRAS showed little effect of RBDv12,
242 and P6T with KRAS G12C showed a stronger effect of the RBDvs on ERK1/2 phosphorylation
243 than on Akt phosphorylation (**Fig. 5A**). P18T with wild-type KRAS showed little effect of
244 either RBDv1 or RBDv12 (**Supplementary Figure 5A**). This is consistent with different cancers
245 having diverse adaptive signaling pathways and different signaling dependencies.
246 Despite the variability in the effects on kinase phosphorylation, subsets of the
247 organoids with mutant Ras (P6T and P28T) and those with wild-type Ras (P17T and P24bT)
248 had reduced viability when expressing either RBDv1 or RBDv12, as indicated by reduced
249 metabolic activity (ATP content) (**Fig. 5B**). In addition, the effect of RBDvs on cell viability
250 correlated with decreased colony size as determined by bright field microscopy (**Fig. 5C**).
251 Importantly, quantification of the colony size indicated that the inhibitory RBDvs significantly
252 reduced growth when compared to non-induced organoids (**Fig. 5D**). However, growth of
253 P18T and P20T, both with wild-type KRAS, and P26T with KRAS G12V was unaffected by
254 either RBDv1 or RBDv12 (**Supplementary Figure 5B**). Thus, KRAS mutant status was
255 insufficient to predict sensitivity to the growth-inhibiting effects of Ras inhibition (**Table 1**).
256 Our data indicated that the RBDvs classify colorectal cancer samples for Ras dependency.
257 The difference in responsiveness to RBDvs was not related to downstream activation of
258 growth signaling by mutant BRAF or PI3K in these organoids, because we tested organoids
259 that are wild-type for BRAF and PI3K[29]. In conclusion, the RBDvs decreased the growth of
260 four patient-derived organoid lines, indicating that inhibiting the interactions between
261 activated Ras proteins and their effectors may be a valid strategy in cancer therapy.
262
263 **Discussion**
264 By engineering the Ras/Raf interface of the CRAF-RBD, we developed potent and highly
265 selective inhibitors of activated Ras that outcompete the binding of signaling effectors. The
266 selectivity of the engineered variants for an active conformation of Ras occurred through
267 molecular contacts to a minimal epitope composed of switch 1 residues at the center of the
268 effector binding site. High affinity was achieved by a subtle rewiring and optimization of the
269 hydrogen bond pattern at the interface between the RBD and HRAS. Because the effector
270 binding site is conserved amongst Ras family members, we detected interactions between
271 the RBDvs and other Ras GTPases with nearly identical sequence composition in the switch 1
272 region. This multispecificity may be beneficial for therapeutic applications based on the

273 RBDvs, because cancer cells often develop resistance to highly specific targeted therapies
274 [30, 31]. The ability to inhibit multiple related Ras family members specifically in the active
275 conformation may prevent a bypass or network rewiring that enables resistance, may
276 interfere with other pathways that collectively provide cancer cells a growth advantage, or
277 may sensitize cancer cells to other therapeutics.

278 In cellular experiments, expression of RBDvs efficiently reduced ERK and AKT
279 phosphorylation and cellular growth and triggered apoptosis in cell lines from different
280 cancer backgrounds. We applied the RBDvs to a clinical research question and showed that
281 the RBDvs could be used as a tool to delineate Ras dependency in colorectal cancer
282 carcinoma (CRC) [29]. In CRC several different signaling pathways have been implicated in
283 disease pathogenesis [32]. However, the extent and heterogeneity of genetic alterations in
284 CRC makes it difficult to analyze the contribution of individual pathways to the proliferative
285 phenotype [29]. More importantly, this diversity makes defining an effective treatment
286 strategy challenging. We showed that the inhibition observed in adherent cell culture
287 experiments translates to patient-derived colorectal cancer organoids: Several of the
288 organoids exhibited reduced growth when expressing either RBDv1 or RBDv12. However,
289 indicative of their varying degree of Ras dependency, not all organoids responded equally
290 well to Ras inhibition by the inhibitory RBDvs. Unexpectedly, the Ras dependency did not
291 correspond to the presence of mutant Ras, showing that genetic information is insufficient
292 to predict therapeutic response. Thus, the RBDvs can be used to facilitate functional
293 classification of Ras dependency in intestinal tumor organoids, which has the potential to
294 drive therapeutic strategies.

295 Although the RBDvs are a unique tool for studying Ras-dependent signaling
296 processes, several intracellular affinity reagents targeting GTP-bound Ras have been
297 reported [13, 15-17]. Compared with the previously reported Ras-targeted reagents, the
298 RBDvs were effective at lower concentrations. For example, the affinity reagent R11.1.6,
299 based on a DNA-binding domain from a thermophilic archaeon, binds Ras in an active
300 conformation and competes with effector binding [15]. Although initial experiments in
301 HEK293T cells suggested otherwise, R11.1.6 does not affect Ras-mediated signaling in a
302 broad range of cancer cell lines [20]. Kauke *et al*. concluded that a higher concentration of
303 R11.1.6 than was achieved by lentiviral transduction is required to efficiently outcompete
304 Ras-binding effectors. Similar observations have been made for intracellular antibodies

305 targeting the Ras-effector binding interface. The antibody fragment iDab#6 required the
306 addition of a membrane localization peptide to overcome the binding avidity of endogenous
307 Ras effectors to inhibit Ras-dependent signaling events [16]. The cell-penetrating TMab4
308 RT11 antibody targeting the switch 1 site of Ras proteins also requires high concentrations to
309 effectively inhibit Ras-mediated signaling events [17]. Two designed ankyrin repeat proteins
310 (DARPins) with specificity for either the GDP-bound inactive state (K27) or the GTP-bound
311 active state (K55) of Ras have been reported [13]. Both DARPins inhibit Ras signaling in
312 transfected HEK293T cells and lentivirus transduced HCT 116 cells; however, it remains to be
313 seen if the observed effects occur in other cell types and organoids. The lower affinity of K55
314 (167 nM) compared with that of CRAF-RBDwt (~ 60-80 nM) for GTP-bound Ras also suggests
315 that a high concentration will be required to compete for endogenous effectors in a cellular
316 context.
317 In contrast to these other Ras interaction inhibitors, the intracellular inhibition of Ras
318 signaling by the RBDvs does not show similar avidity or concentration dependent effects.
319 Indeed, we observed robust inhibition in several different cell lines and organoids despite
320 the expression of the RBDvs was always less than the corresponding wild-type control. The
321 RBDvs exhibited preferential binding to active Ras proteins, indicating high selectivity not
322 only for Ras proteins with a shared effector binding site but also for these proteins in their
323 active conformation. Most likely, the other interaction inhibitors, especially TMab4 RT11
324 that also binds the switch-1 sequence, may also have similar multispecificity for Ras proteins.
325 This potential property of the other affinity reagents should be further examined.
326 A common challenge in all these efforts is the effective delivery of intracellular
327 affinity reagents to the cytosol. Consequently, various intracellular protein delivery
328 platforms, such as cell-penetrating peptides, nanocarrier, liposomes, polymer and
329 nanoparticle-stabilized nanocapsules (reviewed in [33]), are actively under investigation.
330 Another promising strategy for the delivery of proteins into mammalian cells is the use of
331 bacterial toxins, which can deliver a wide array of passenger proteins spanning a range of
332 sizes, structures, and stabilities[34]. For example, a recent report shows that a fusion protein
333 of the RBDwt is able to pass through the channel of a tripartite toxin complex (Tc toxins)
334 derived from bacterial pathogens. Thus, due to its small size and favorable charge
335 distribution the RBD-scaffold may be particularly suited for delivery by Tc toxins [35]. In
336 future, these and other platforms can enable targeted delivery of proteins into cells to

337 realize the potential of protein-based therapeutics with intracellular sites of action. RBDvs
338 would then be a candidate for delivery to test in treating diseases associated with
339 unchecked Ras activity.

340 **Material and Methods**

341 **Ras expression, purification and nucleotide exchange**

342 The human HRAS (AA 1-166) and KRAS (AA 1-169, isoform B) proteins were expressed as GST-
343 fusions from pGEX-6P-1 plasmids for selection experiments and as His-tag fusions from pET-
344 53 plasmids for *in vitro* competition and binding assays. Plasmids were used to transform *E.*
345 *coli* Rosetta(DE3) cells and individual colonies were handled essentially as written before [22],
346 except that all buffers were supplemented with 5 mM $MgCl_2$. Briefly, resulting cultures from
347 individual colonies were inoculated into Luria Broth (LB) media and protein expression was
348 induced at OD_{600}=0.8 with 0.5 mM IPTG. After overnight incubation at 16 °C, bacterial pellets
349 were resuspended in 50 mM Tris-HCl pH 7.5, 150 mM NaCl, 1 mM PMSF and 5 mM $MgCl_2$ and
350 lysed by sonication. The lysates were clarified by centrifugation and proteins in the
351 supernatant were purified using Ni-NTA chromatography (Qiagen) for His-tagged proteins or
352 Glutathione Sepharose 4 Fast Flow beads (GE Healthcare) for GST-tagged proteins at 4 °C
353 following the manufacturer's instructions. Eluted fractions were dialyzed into 150 mM NaCl,
354 50 mM Tris-HCl pH 7.5, 1 mM DTT and 5 mM $MgCl_2$ and protein concentrations were
355 determined by measuring the absorption at 280 nm. Nucleotide exchange to GTPγS or GDP
356 was performed by the addition of 10-fold molar excess of GTPγS or GDP (Sigma Aldrich) and 5
357 mM EDTA to dialyzed proteins. After 30 min incubation at 37 °C, proteins were transferred on
358 ice and exchange was quenched by the addition of 10 mM $MgCl_2$ final concentration.

359

360 **Construction of a phage-displayed CRAF-RBD library**

361 For phage library construction, Ras-binding domain (RBD) of human CRAF kinase (AA 55-131)
362 was cloned into the phagemid pNE [21] and cysteines at position 81, 95 and 96 of the RBD
363 were mutated to serines using site-directed mutagenesis [36]. Afterwards, two degenerate
364 oligonucleotides were used to introduce mutations at 2 regions of the RBD gene by site-
365 directed mutagenesis. Oligonucleotides were soft-randomized as described before [21, 22].
366 The nucleotide ratio was adjusted to 70 % of the wt nucleotide represented N1 = A, N2 = C,
367 N3 = G and N4 = T and 10 % of each of the other three nucleotides.

368 Oligonucleotide 1: GAT GAC AAA AGC AAC N1N2N4 ATC N2N3N4 GTT N4N4N2 TTG CCG AAC
369 N1N1N3 N2N1N1 N1N3N1 ACA N3N4N3 GTC N1N1N4 GTG CGA AAT GGA ATG

370 Oligonucleotide 2: CAT GAC TGC CTT ATG N1N1N1 N3N2N1 CTC N1N1N3 N3N4N3 N2N3N3
371 N3N3N2 CTG CAG CCA GAG TGC

372 The resulting library was used to electroporate *E. coli* SS320 cells using established methods
373 resulting in $2.2x10^9$ independent RBD variants [37].
374
375 **RBD variant selection against activated HRAS**
376 Library pool of phage displaying individual RBD variants were harvested by precipitation with
377 PEG/NaCl (20 % PEG-8000 (w/v), 2.5 M NaCl) and resuspended in PBT buffer (1x PBS, 1 %
378 BSA, 0.1 % Tween 20) supplemented with 5 mM $MgCl_2$. Immobilization of GTPγS-loaded GST-
379 tagged HRAS and subsequent binding selections were done essentially as described before
380 [22], except that all buffers were supplemented with 5 mM $MgCl_2$. In brief, 4 wells of a 96
381 well Maxisorp microtiter plate (NUNC) were coated with 100 µl of 2 µM GST-tagged GTPγS-
382 loaded HRAS in dialysis buffer (150 mM NaCl, 50 mM Tris-HCl pH 7.5, 1 mM DTT and 5 mM
383 $MgCl_2$) over night at 4 °C. After blocking with PBT buffer for 1 h, phage library pool was
384 added to each well and incubated for 1 hour at 4 °C. The plate was washed 8 times with cold
385 PT buffer (1x PBS, 0.1 % Tween 20) and bound phage were eluted with 0.1 M HCl and
386 immediately neutralized with 1.0 M Tris-HCl pH 8.0. Eluted phage were directly used to
387 infect exponentially growing *E. coli* XL1-blue supplemented with helper phage M13K07 (NEB)
388 and incubated over night at 37 °C. In each successive selection round, the selection
389 stringency was increased by 2 additional washing steps and. To avoid unspecific binding
390 towards the GST-tag, a GST counter-selection was performed starting with round 2.
391 Additionally, after 3 rounds of selection, phage binding and washing was done at room
392 temperature and the concentration of coated GST-tagged GTPγS-loaded HRAS was reduced
393 to 0.5 µM. After five rounds of enrichment, individual RBD variants with improved binding
394 properties towards active HRAS were identified by clonal phage ELISA as described [37]. In
395 brief, phage displaying individual RBD variants were prepared from single colonies of
396 bacteria harboring phagemids encoding RBDvs and transferred to 384-well Maxisorp plates
397 immobilized with GST-tagged GTPγS-labelled HRAS (0.5 µM) and blocked with BSA, as
398 described previously. As negative controls, wells were coated with GST or only blocked with
399 BSA. After incubation, washing and developing, positive clones were further analysed by
400 sequencing.
401
402 **Cloning of RBD variants**

403 DNA fragments encoding the selected variants and the unmodified RBDwt were cloned into
404 pDONR233 plasmids by Gateway cloning (Invitrogen) as described before [22]. Further
405 recombination into the Gateway destination vectors pET53DEST, pDEST15 and pLDT-NT-HA
406 was performed according to the manufacturer's instructions (Invitrogen).
407
408 **RBDvs protein expression and purification**
409 For competitive *in vitro* pull-down experiments and bio-layer interferometry measurements,
410 His-tagged (from pET53DEST plasmids) and GST-tagged (from pGEX-6p-1 plasmids) RBD
411 variants and RBDwt, Ras-association domain (RA) of RalGDS (AA 798-885) and GST alone were
412 processed as Ras proteins (see above).
413
414 **Competitive *in vitro* pull-down experiment**
415 The Ras/RBDwt competition assay was performed in 200 µl assay buffer (25 mM Tris-HCl pH
416 7.5, 150 mM NaCl, 1 % NP-40, 5 mM $MgCl_2$ and 5 % glycerol) using 8 µg (1.15 µM) GST-tagged
417 RBDwt or RalGDS-RA bound to GSH-sepharose beads. First, 5 µg (1.15 µM) of His-tagged KRAS
418 loaded with GTPγS was incubated with His-tagged RBDwt or RBDvs with increasing
419 concentrations (2.3 µg [1.15 µM], 5.8 µg [2.68 µM] and 23 µg [11.5 µM], which corresponds
420 to a molar ratio of 1:1, 1:2.5 and 1:10 of GST-tagged RBDwt or RalGDS-RA:His-tagged RBDwt
421 or RBDvs) for 30 min at 4 °C with end-over-end rotation. 8 µg of beads were added to the
422 reaction mix and incubated for another 30 min at 4 °C. After 2 washes with assay buffer, beads
423 were resuspended in 30 µl 2x SDS sample buffer and incubated for 5 min at 95 °C. Controls
424 samples consisted of GTPγS- or GDP-loaded KRAS incubated with GST-RBDwt or GST-RalGDS-
425 RA beads. Also, GTPγS-loaded KRAS was incubated with GST bound to beads. Samples were
426 analyzed by immunoblot using anti-Ras antibody (#16117 ThermoFischer Scientific) and
427 membrane was stained with Ponceau S as loading control.
428
429 **Bio-layer interferometry (BLI)**
430 Kinetic binding assays were performed on Octet RED96 instrument (Pall ForteBio). Dialyzed
431 proteins were supplemented with 0.1 % BSA and 0.02 % Tween 20. GST or GST-tagged RBDvs
432 were immobilized onto anti-GST biosensors (Pall ForteBio) at a concentration of 2 µg/ml.
433 Association was analyzed at concentrations starting from 1000 nM to 15.6 nM in 1:1 dilution
434 steps of GTPγS- or GDP-loaded HRAS. Dissociation was measured in dialysis buffer (150 mM

435 NaCl, 50 mM Tris-HCl pH 7.5, 1 mM DTT and 5 mM $MgCl_2$) supplemented with 0.1 % BSA and
436 0.02 % Tween 20. Non-specific interaction of HRAS with biosensors was assayed using empty
437 anti-GST sensors. Reference wells were subtracted from sample wells and a 1:1 global fitting
438 model was used to determine k_{on}, k_{off} and K_d values.
439
440 **Protein expression and purification for crystallography**
441 RBDv1, RBDv12 and HRAS G12V (residues 1-166) were expressed as TEV protease cleavable
442 GST-fusions using a modified pGEX-2T vector. Expression constructs were transformed into
443 BL21-CodonPlus DE3-RIL bacteria (Agilent Technologies) for protein production. Bacterial
444 expression was induced overnight at 18 °C with 0.5 mM IPTG and was performed in LB media.
445 RBDvs bacterial pellets were resuspended in 50 mM HEPES pH 7.5, 300 mM NaCl, 5 % glycerol,
446 1 mM PMSF, 1 mM TCEP and lysed by homogenization. The lysate was cleared by
447 centrifugation at 4 °C for 40 minutes at 18,000 g. Protein was bound to glutathione affinity
448 resin (GE Healthcare), eluted by cleavage of the GST-tag with TEV, concentrated and then
449 buffer exchanged by size exclusion chromatography (SEC) using a Superdex75 24 ml column
450 (GE healthcare) equilibrated in 50 mM HEPES pH 7.5, 50 mM NaCl, 5 % glycerol, 10 mM $MgCl_2$,
451 1 mM TCEP.
452 HRAS G12V bacterial pellets were resuspended in 50 mM HEPES pH7.5, 300 mM NaCl, 5 mM
453 EDTA, 5 % glycerol, 1 mM PMSF, 1 mM TCEP and lysed by homogenization. The lysate was
454 clarified by centrifugation at 4 °C for 40 minutes at 18,000 g. Protein was bound to glutathione
455 affinity resin (GE Healthcare), washed with 50 mM HEPES pH 7.5, 300 mM NaCl, 25 mM
456 imidazole, 5 % glycerol, 1 mM TCEP and eluted by cleavage of the GST-tag with TEV,
457 concentrated and then buffer exchanged by SEC using a Superdex75 24 ml column
458 equilibrated in 50 mM HEPES pH7.5, 300 mM NaCl, 5 mM EDTA, 5 % glycerol, 1 mM TCEP.
459 GMP-PNP loading on HRAS G12V was carried out by incubating purified HRAS G12V with 10-
460 fold excess of GMP-PNP for 80 min at 4 ˚C followed by the addition of 30-fold excess of $MgCl_2$
461 for 120 min at 4 ˚C.
462 The RBDvs:HRAS G12V complexes were obtained by mixing RBDvs and GMP-PNP loaded HRAS
463 G12V at equal molar ratio for 60 min at 4 ˚C followed by SEC using a Superdex75 24 ml column
464 equilibrated in 50 mM HEPES pH 7.5, 50 mM NaCl, 10 mM $MgCl_2$, 5 % glycerol, 1 mM TCEP. All
465 fractions corresponding to co-elution of HRAS G12V with RBDvs were pooled and
466 concentrated to 12.2 mg/ml, then flash frozen in liquid nitrogen. Protein concentration was

467 estimated by UV-Vis absorption spectroscopy using a NanoDrop spectrophotometer (Thermo-
468 Fisher Scientific).
469
470 **Protein crystallography, data collection and structural analysis.**
471 The RBDvs:HRAS G12V complexes were crystallized at 20 ˚C in sitting-drop by mixing 0.5 µL of
472 complexes (450 µM, 12.2 mg/ml) with 0.5 µL of mother liquor of 0.1 M sodium cacodylate pH
473 6.5, 200 mM ammonium sulphate, 30 % PEG 4000 or mother liquor of 0.1 M sodium citrate
474 pH 5.6, 200 mM ammonium sulphate, 30 % PEG 4000 for RBDv1:HRAS G12V and RBDv12:HRAS
475 G12V, respectively. X-ray diffraction data were collected on a flash-frozen crystal cryo-
476 protected in mother liquor containing 25 % glycerol at 100 K on station 24-ID-C, NE CAT
477 beamline, Advanced Photon Source (APS). Data reduction was performed using XDS package
478 [38]. The structure was solved by molecular replacement using PDB 4G0N [5] as a search
479 model in Phaser [39]. Model building and refinement was performed using COOT [40],
480 LORESTR [41] and REFMAC [42] from the CCP4 suite [43]. The data statistics and refinement
481 details are reported in Supplementary Table 1.
482
483 **Cell culture**
484 HCT 116 (#CCL-247) cells were purchased from ATCC and handled according to the supplier's
485 instructions. MIA PaCa-2, A549 and H1299 cell lines were cultured in DMEM (MIA PaCa-2 and
486 A549) or RPMI-1640 (H1299) medium (both Gibco) supplemented with 10% (v/v) fetal bovine
487 serum (Gibco). Cell lines were tested and found to be mycoplasma-free. Lenti viral particles
488 were produced in HEK293T cells using established protocols [44]. Stable cell lines were
489 constructed using lentiviral vectors (pLDT) encoding N-terminally HA-tagged RBDvs and wt
490 under the control of a doxycycline inducible promotor by standard techniques [45]. The
491 original pLDT plasmid was a gift from Jason Moffat (University of Toronto, The Donnelly
492 Centre, 160 College St., Toronto). Two days after transduction, cell lines were selected with 2
493 µg/ml puromycin for HCT 116, MIA PaCa-2, A549 and H1299. For all experiments, 1 µg/ml
494 doxycycline was used to induce expression of HA-tagged RBDvs or RBDwt.
495
496 **Immunoprecipitation for mass spectrometry**
497 Two 10 cm dishes per construct (RBDwt, v1 and v12) were seeded with $2x10^6$/ml stable HCT
498 116 cells and RBDvs expression was induced 24 h later with doxycycline. After 24 h induction,

499 cells were scraped into 1x PBS and washed twice with 1x PBS. After centrifugation, the cell
500 pellets were resuspended in lysis buffer (25 mM Tris-HCl pH 7.5, 150 mM NaCl, 1 % NP-40, 5
501 mM $MgCl_2$, 5 % glycerol and protease inhibitor cocktail [Roche]) and incubated for 20 min at
502 4 °C with end-over-end rotation. The lysates were centrifuged, supernatants were transferred
503 to 20 µl pre-equilibrated anti-HA affinity matrix (Roche) and incubated for 40 min at 4 °C.
504 Beads were washed 2 times with 500 µl lysis buffer. Elution was performed by the addition of
505 20 µl 2x SDS-sample buffer to the beads and incubation for 3 min at 95 °C. 5 µl of samples
506 were analysed by immunoblotting using antibodies against endogenous Ras, HA-tag and
507 GAPDH (#3965, #2999 and #8884, respectively; all from Cell Signaling Technology). Sample
508 preparation for in-gel digest was done as described before [46]. In brief, supernatants were
509 loaded onto SDS-polyacrylamide gel and the gel was stained using InstantBlue (Expedeon). Gel
510 lanes were cut into pieces and subsequently washed, destained and dehydrated. Proteins
511 were reduced with 10 mM dithiothreitol (DTT), alkylated with 55 mM iodoacetamide (IAA)
512 and digested overnight with sequencing-grade Trypsin (Promega). Peptides were extracted
513 using an increasing concentration of acetonitrile. Finally, peptides were concentrated and
514 desalted using the Stop and Go Extraction (STAGE) technique [47].
515
516 **Liquid chromatography and mass spectrometry**
517 A binary buffer system consisting of buffer A (0.1 % formic acid) and buffer B (80 % acetonitrile,
518 0.1 % formic acid) was used for peptide separation on an Easy-nLC 1200 (Thermo Fisher
519 Scientific). This system was coupled *via* a nano electrospray ionization source to the
520 quadrupole-based Q Exactive HF benchtop mass spectrometer [48]. Peptide elution from the
521 in-house packed 18 cm (1.9 µm C18 Beads, Dr. Maisch, Germany) column was achieved by
522 increasing the relative amount of B from 10 % to 38 % in a linear gradient within 23 min at a
523 column temperature of 40 °C. Followed by an increase to 100 % B within 7 min, gradients were
524 completed by a re-equilibration to 5 % B.
525 Q Exactive HF settings: MS spectra were acquired using 3E6 as an AGC target, a maximal
526 injection time of 20 ms and a 60,000 resolution at 300 m/z. The mass spectrometer operated
527 in a data dependent Top15 mode with subsequent acquisition of higher-energy collisional
528 dissociation (HCD) fragmentation MS/MS spectra of the top 15 most intense peaks. Resolution
529 for MS/MS spectra was set to 30,000 at 200 m/z, AGC target to 1E5, maximal injection time
530 to 64 ms and the isolation window to 1.6 Th.

531

532 **Mass spectrometry data processing and analysis**

533 All acquired raw files were processed using MaxQuant (1.5.3.30) [49] and the implemented
534 Andromeda search engine [50]. For protein assignment, electrospray ionization-tandem mass
535 spectrometry (ESI-MS/MS) fragmentation spectra were correlated with the Uniprot human
536 database (v. 2016) including 4 manually added sequences of the RBD variants and KRAS G13D
537 (RBDwt: MGYPYDVPDYAGQGPDPSTNSADITSLYK
538 KAGFSNTIRVFLPNKQRTVVNVRNGMSLHDCLMKALKVRGLQPECCAVFRLLHEHKGKKARLDWNTDA
539 ASLIGEELQVDFL; RBDv1: MGYPYDVPDYAGQGPDPSTNSADIT
540 SLYKKAGFSNTIRVLLPNQEWTVVKVRNGMSLHDSLMKALKRHGLQPESSAVFRLLHEHKGKKARLDW
541 NTDAASLIGEELQVDFL; RBDv12: MGYPYDVPDYAGQGPDPST
542 NSADITSLYKKAGFSNTIRVLLPNHERTVVKVRNGMSLHDSLMKALKRHGLQPESSAVFRLLHEHKGKKA
543 RLDWNTDAASLIGEELQVDFL; KRAS G13D: MTEYKLVVVGAGD
544 VGKSALTIQLIQNHFVDEYDPTIEDSYRKQVVIDGETCLLDILDTAGQEEYSAMRDQYMRTGEGFLCVFAI
545 NNTKSFEDIHHYREQIKRVKDSEDVPMVLVGNKCDLPSRTVDTKQAQDLARSYGIPFIETSAKTRQGVDD
546 AFYTLVREIRKHKEKMSKDGKKKKKKSKTKCVIM). Searches were performed with tryptic
547 specifications and default settings for mass tolerances for MS and MS/MS spectra.
548 Carbamidomethyl at cysteine residues was set as a fixed modification, while oxidation at
549 methionine and acetylation at the N-terminus were defined as variable modifications. The
550 minimal peptide length was set to seven amino acids and the false discovery rate for proteins
551 and peptide-spectrum matches to 1 %. The match-between-run feature was used with a time
552 window of 0.7 min. Relative label-free quantification of proteins was done using the MaxLFQ
553 algorithm integrated into MaxQuant [51]. The minimum LFQ ratio count was set to 2 and the
554 FastLFQ option was enabled.

555 For subsequent analysis, the Perseus software (1.5.3.0) [52] was used and first filtered for
556 contaminants and reverse entries and proteins that were only identified by site. The LFQ
557 intensities were logarithmized to base 2 and grouped into duplicates. To overcome the missing
558 value problem in immunoprecipitation data, proteins that were quantified less than 2 times
559 in one of the experimental groups were discarded from further analysis. Missing values were
560 imputed column-wise by a down-shifted (median-1.8) Gaussian distribution mimicking the
561 detection limit of the mass spectrometer.

562

563 **Metabolic activity assay**

564 1000 cells of each stable cell line were seeded in a 96 well plate in duplicates. The following
565 day, expression was induced by the addition of doxycycline. Corresponding control wells were
566 not induced. Cell viability was assayed 120 h after induction using CellTiter-Glo (Promega).
567 Luminescence signals of induced wells were normalized to uninduced well data.

568

569 **Immunoblotting**

570 Stable cell lines were seeded in 6 well plates (1×10^5 cells/well) and induced 24 h later with
571 doxycycline (1µg/ml). Control cells were left uninduced. 24 h after induction, cells were
572 washed twice with 1x PBS and lysed in 200 µl 2x SDS sample buffer. Whole cell lysates were
573 analyzed by immunoblot using the indicated antibodies. For serum starvation experiments,
574 medium was replaced upon induction with serum-free medium. 24 h after induction, cells
575 were treated with 100 ng/ml EGF (Sigma) for 10 min before lysis.

576

577 **Antibodies**

578 Antibodies used for western blot analysis were: pospho-ERK1/2 (p44/42 MAPK)
579 (Thr202/Tyr204) (clone D13.14.4E #4370), ERK1/2 (p44/42 MAPK) (clone 137F5 #4695),
580 phospho-AKT (Ser473) (clone D9E #4060), AKT (clone C67E7 #4691), GAPDH-HRP (clone
581 D16H11 #8884), and HA-HRP (clone 6E2 #2999) were purchased from Cell Signaling
582 Technologies.

583

584 **Analysis of cell growth by real-time cell analysis (RTCA)**

585 Cell proliferation of stably transduced HCT 116 cells was assessed using xCELLigence real-time
586 cell analysis (RTCA) SP (single plate) system (ACEA Biosciences). 1000 cells/well were seeded
587 in a 96-well electronic microtiter plate (ACEA Biosciences) with 200 µl medium/well. After
588 24 h, cells were induced by doxycycline. Cell proliferation was monitored for 120 h.
589 Experiments were performed as duplicates and repeated at least twice.

590

591 **Apoptosis analysis by flow cytometry**

592 Stably transduced HCT 116 cells were seeded in 6-well plates (1×10^5 cells/well) and induced
593 24 h later with doxycycline. Control cells were left uninduced. After 72 h, cells were washed
594 once with 1x PBS. For analysis of apoptotic cells, Annexin V-FITC apoptosis detection kit (#ALX-

595 850-020 Enzo) was used following the manufacturer's protocol. Samples were analyzed on a
596 FACSCanto II flow cytometer (BD Biosciences) and data were processed by FlowJo software
597 (FlowJo, LLC). Gating was done based on viable and single cells that were identified on the
598 basis of scatter morphology.
599
600 **Organoid cultures**
601 Human tumor colon organoid samples were obtained from a published colorectal cancer
602 organoid biobank [29]. Resection tissues were obtained with written informed consent, and
603 following approval by the ethics committees of the Diakonessen Hospital, Utrecht. Tissue was
604 obtained with written informed consent and following approval, according to the guidelines
605 of the University Cancer Center (UCT), Frankfurt. Organoid cultures were established and
606 maintained as described previously [53]. Tumor organoids were maintained in medium lacking
607 Wnt3a. The organoid lines were transduced as described [54] with lentivirus expressing N-
608 terminally HA-tagged RBDwt, RBDv1 or RBDv12 (as above). Three days after transduction,
609 organoids were selected with 1 µg/mL puromycin in the culture medium. For cell viability
610 assays, the cells were seeded in Matrigel either following mechanical dissociation or
611 enzymatic single cell dispersal using TrypLE Express reagent (Gibco). 2 µg/mL doxycycline was
612 added 1 day after seeding. After 3 days cell viability was measured using CellTiter-Glo reagent
613 (Promega). All experiments were measured as technical triplicates and the experiments were
614 repeated at least twice each.
615 For quantification of organoid size, light microscopy pictures were taken at a 2x resolution
616 after 2-6 days of doxycycline exposure, as indicated. The diameter (µm) of all viable organoids
617 in one picture of each condition was measured using ImageJ. Viable organoids were identified
618 as refringent, while dark structures surrounded by cell debris were excluded from the analysis.
619 The quantification was performed on two independent experiments.
620
621 **Statistical methods**
622 Data are presented as the mean ± standard deviation (SD). The comparisons between RBDwt
623 and RBDvs were made by an unpaired t test using GraphPad Prism software. For statistical
624 analysis of the quantification results of organoid sizes, a Mann-Whitney U-test was
625 performed using GraphPad Prism software. The level of significance was set at $^{*}P < 0.05$, $^{**}P <$
626 0.01 and $^{***}P < 0.005$.

Acknowledgments:

This work was supported by LOEWE Ub-Net, Cluster of Excellence "Macromolecular Complexes" (DFG EXC115), and the Collaborative Research Center SFB 1177. We thank Mani Ravichandran from the Structural and Genomic Consortium (SGC) of Toronto for providing X-Ray crystallography screening kits. This work was supported by funds from an Impact Grant (704116 to F.S.) from the Canadian Cancer Society Research Institute and by operating funds (FDN143277 to F.S.) from the Canadian Institutes for Health Research. P.M. was supported by a TD Bank postdoctoral fellowship. F.S. holds a Canada Research Chair (Tier 1) in Structural Biology of Cell Signaling. K.R. is a Heisenberg professor of the DFG (RA1739/4-2). Diffraction work conducted at the Northeastern Collaborative Access Team beamlines was funded by the National Institute of General Medical Sciences from the National Institutes of Health (P41 GM103403) and by an NIH-ORIP HEI grant (S10 RR029205). We thank Nancy R. Gough (BioSerendipity, LLC) for constructive comments and editorial assistance. We thank Jason Moffat (University Toronto) for donation of inducible lentiviral plasmids.

Author contributions:

S.W. and A.E. designed the study, designed the RBD library, analyzed the data and wrote the manuscript. S.W. performed library construction and selection, *in vitro* competition experiments, binding experiments and all cellular experiments. P.M and I.K. performed structural studies and P.M., F.S., S.W. and A.E. analyzed structural data. S.W. performed Co-IP and MS and S.W., M.H. and A.E. analyzed MS data. K.R. contributed to the design, provided reagents and analyzed data. M.B.G. performed organoid experiments and M.B.G., H.F.F., S.W., H.C. and A.E. analyzed organoid data. M.K. analyzed data and provided reagents.

Conflict of interest

The authors declare no competing interests.

Data and materials availability:

All data is available in the main text or the supplementary materials. All data and material will be made available upon request.

660 **References**

661 1. Weber CK, Slupsky JR, Kalmes HA, Rapp UR (2001) Active Ras induces
662 heterodimerization of cRaf and BRaf. *Cancer Res* **61**: 3595-8
663 2. Vossler MR, Yao H, York RD, Pan MG, Rim CS, Stork PJ (1997) cAMP activates MAP
664 kinase and Elk-1 through a B-Raf- and Rap1-dependent pathway. *Cell* **89**: 73-82
665 3. York RD, Yao H, Dillon T, Ellig CL, Eckert SP, McCleskey EW, Stork PJ (1998) Rap1
666 mediates sustained MAP kinase activation induced by nerve growth factor. *Nature* **392**: 622-
667 6
668 4. Yuryev A, Ono M, Goff SA, Macaluso F, Wennogle LP (2000) Isoform-specific
669 localization of A-RAF in mitochondria. *Mol Cell Biol* **20**: 4870-8
670 5. Fetics SK, Guterres H, Kearney BM, Buhrman G, Ma B, Nussinov R, Mattos C (2015)
671 Allosteric effects of the oncogenic RasQ61L mutant on Raf-RBD. *Structure* **23**: 505-16
672 6. Nassar N, Horn G, Herrmann C, Scherer A, McCormick F, Wittinghofer A (1995) The
673 2.2 A crystal structure of the Ras-binding domain of the serine/threonine kinase c-Raf1 in
674 complex with Rap1A and a GTP analogue. *Nature* **375**: 554-60
675 7. Nakhaeizadeh H, Amin E, Nakhaei-Rad S, Dvorsky R, Ahmadian MR (2016) The RAS-
676 Effector Interface: Isoform-Specific Differences in the Effector Binding Regions. *PLoS One* **11**:
677 e0167145
678 8. John J, Sohmen R, Feuerstein J, Linke R, Wittinghofer A, Goody RS (1990) Kinetics of
679 interaction of nucleotides with nucleotide-free H-ras p21. *Biochemistry* **29**: 6058-65
680 9. Rudolph MG, Linnemann T, Grunewald P, Wittinghofer A, Vetter IR, Herrmann C
681 (2001) Thermodynamics of Ras/effector and Cdc42/effector interactions probed by
682 isothermal titration calorimetry. *J Biol Chem* **276**: 23914-21
683 10. Cox AD, Fesik SW, Kimmelman AC, Luo J, Der CJ (2014) Drugging the undruggable
684 RAS: Mission possible? *Nat Rev Drug Discov* **13**: 828-51
685 11. Spencer-Smith R, Koide A, Zhou Y, Eguchi RR, Sha F, Gajwani P, Santana D, Gupta A,
686 Jacobs M, Herrero-Garcia E*, et al.* (2017) Inhibition of RAS function through targeting an
687 allosteric regulatory site. *Nat Chem Biol* **13**: 62-68
688 12. Khan I, Spencer-Smith R, O'Bryan JP (2018) Targeting the alpha4-alpha5 dimerization
689 interface of K-RAS inhibits tumor formation in vivo. *Oncogene*

690 13. Guillard S, Kolasinska-Zwierz P, Debreczeni J, Breed J, Zhang J, Bery N, Marwood R,
691 Tart J, Overman R, Stocki P*, et al.* (2017) Structural and functional characterization of a
692 DARPin which inhibits Ras nucleotide exchange. *Nat Commun* **8**: 16111
693 14. McGee JH, Shim SY, Lee SJ, Swanson PK, Jiang SY, Durney MA, Verdine GL (2018)
694 Exceptionally high-affinity Ras binders that remodel its effector domain. *J Biol Chem* **293**:
695 3265-3280
696 15. Kauke MJ, Traxlmayr MW, Parker JA, Kiefer JD, Knihtila R, McGee J, Verdine G,
697 Mattos C, Wittrup KD (2017) An engineered protein antagonist of K-Ras/B-Raf interaction.
698 *Sci Rep* **7**: 5831
699 16. Tanaka T, Williams RL, Rabbitts TH (2007) Tumour prevention by a single antibody
700 domain targeting the interaction of signal transduction proteins with RAS. *EMBO J* **26**: 3250-
701 9
702 17. Shin SM, Choi DK, Jung K, Bae J, Kim JS, Park SW, Song KH, Kim YS (2017) Antibody
703 targeting intracellular oncogenic Ras mutants exerts anti-tumour effects after systemic
704 administration. *Nat Commun* **8**: 15090
705 18. Filchtinski D, Sharabi O, Ruppel A, Vetter IR, Herrmann C, Shifman JM (2010) What
706 makes Ras an efficient molecular switch: a computational, biophysical, and structural study
707 of Ras-GDP interactions with mutants of Raf. *J Mol Biol* **399**: 422-35
708 19. Trinh TB, Upadhyaya P, Qian Z, Pei D (2016) Discovery of a Direct Ras Inhibitor by
709 Screening a Combinatorial Library of Cell-Permeable Bicyclic Peptides. *ACS Comb Sci* **18**: 75-
710 85
711 20. Kauke MJ, Tisdale AW, Kelly RL, Braun CJ, Hemann MT, Wittrup KD (2018) A Raf-
712 competitive K-Ras binder can fail to functionally antagonize signaling. *Mol Cancer Ther*
713 21. Ernst A, Avvakumov G, Tong J, Fan Y, Zhao Y, Alberts P, Persaud A, Walker JR, Neculai
714 AM, Neculai D*, et al.* (2013) A strategy for modulation of enzymes in the ubiquitin system.
715 *Science* **339**: 590-5
716 22. Wiechmann S, Gartner A, Kniss A, Stengl A, Behrends C, Rogov VV, Rodriguez MS,
717 Dotsch V, Muller S, Ernst A (2017) Site-specific inhibition of the small ubiquitin-like modifier
718 (SUMO)-conjugating enzyme Ubc9 selectively impairs SUMO chain formation. *J Biol Chem*
719 **292**: 15340-15351
720 23. Campbell-Valois FX, Tarassov K, Michnick SW (2005) Massive sequence perturbation
721 of a small protein. *Proc Natl Acad Sci U S A* **102**: 14988-93

722 24. Kiel C, Filchtinski D, Spoerner M, Schreiber G, Kalbitzer HR, Herrmann C (2009)
723 Improved binding of raf to Ras.GDP is correlated with biological activity. *J Biol Chem* **284**:
724 31893-902
725 25. Erijman A, Shifman JM (2016) RAS/Effector Interactions from Structural and
726 Biophysical Perspective. *Mini Rev Med Chem* **16**: 370-5
727 26. Kiel C, Serrano L, Herrmann C (2004) A detailed thermodynamic analysis of
728 ras/effector complex interfaces. *J Mol Biol* **340**: 1039-58
729 27. Fridman M, Maruta H, Gonez J, Walker F, Treutlein H, Zeng J, Burgess A (2000) Point
730 mutants of c-raf-1 RBD with elevated binding to v-Ha-Ras. *J Biol Chem* **275**: 30363-71
731 28. Burgess MR, Hwang E, Mroue R, Bielski CM, Wandler AM, Huang BJ, Firestone AJ,
732 Young A, Lacap JA, Crocker L*, et al.* (2017) KRAS Allelic Imbalance Enhances Fitness and
733 Modulates MAP Kinase Dependence in Cancer. *Cell* **168**: 817-829 e15
734 29. van de Wetering M, Francies HE, Francis JM, Bounova G, Iorio F, Pronk A, van Houdt
735 W, van Gorp J, Taylor-Weiner A, Kester L*, et al.* (2015) Prospective derivation of a living
736 organoid biobank of colorectal cancer patients. *Cell* **161**: 933-45
737 30. Karimkhani C, Gonzalez R, Dellavalle RP (2014) A review of novel therapies for
738 melanoma. *Am J Clin Dermatol* **15**: 323-37
739 31. Manzano JL, Layos L, Buges C, de Los Llanos Gil M, Vila L, Martinez-Balibrea E,
740 Martinez-Cardus A (2016) Resistant mechanisms to BRAF inhibitors in melanoma. *Ann Transl*
741 *Med* **4**: 237
742 32. Fearon ER (2011) Molecular genetics of colorectal cancer. *Annu Rev Pathol* **6**: 479-
743 507
744 33. Fu A, Tang R, Hardie J, Farkas ME, Rotello VM (2014) Promises and pitfalls of
745 intracellular delivery of proteins. *Bioconjug Chem* **25**: 1602-8
746 34. Auger A, Park M, Nitschke F, Minassian LM, Beilhartz GL, Minassian BA, Melnyk RA
747 (2015) Efficient Delivery of Structurally Diverse Protein Cargo into Mammalian Cells by a
748 Bacterial Toxin. *Mol Pharm* **12**: 2962-71
749 35. Roderer D, Schubert E, Sitsel O, Raunser S (2019) Towards the application of Tc toxins
750 as a universal protein translocation system. *bioRxiv*: 706333
751 36. Kunkel TA (1985) Rapid and efficient site-specific mutagenesis without phenotypic
752 selection. *Proc Natl Acad Sci U S A* **82**: 488-92

753 37. Fellouse FA, Sidhu, S.S (2007) *Making antibodies in bacteria.* In Making and using
754 antibodies (G C Howard & M R Kaser, Eds), pp 157–180. CRC Press, Boca Raton, FL
755 38. Kabsch W (2010) Xds. *Acta Crystallogr D Biol Crystallogr* **66**: 125-32
756 39. McCoy AJ, Grosse-Kunstleve RW, Adams PD, Winn MD, Storoni LC, Read RJ (2007)
757 Phaser crystallographic software. *J Appl Crystallogr* **40**: 658-674
758 40. Emsley P, Cowtan K (2004) Coot: model-building tools for molecular graphics. *Acta*
759 *Crystallogr D Biol Crystallogr* **60**: 2126-32
760 41. Kovalevskiy O, Nicholls RA, Murshudov GN (2016) Automated refinement of
761 macromolecular structures at low resolution using prior information. *Acta Crystallogr D*
762 *Struct Biol* **72**: 1149-1161
763 42. Murshudov GN, Vagin AA, Dodson EJ (1997) Refinement of macromolecular
764 structures by the maximum-likelihood method. *Acta Crystallogr D Biol Crystallogr* **53**: 240-55
765 43. Winn MD, Ballard CC, Cowtan KD, Dodson EJ, Emsley P, Evans PR, Keegan RM,
766 Krissinel EB, Leslie AG, McCoy A*, et al.* (2011) Overview of the CCP4 suite and current
767 developments. *Acta Crystallogr D Biol Crystallogr* **67**: 235-42
768 44. Addgene (2016) lentivirus-production. In
769 45. Tiscornia G, Singer O, Verma IM (2006) Production and purification of lentiviral
770 vectors. *Nat Protoc* **1**: 241-5
771 46. Shevchenko A, Tomas H, Havlis J, Olsen JV, Mann M (2006) In-gel digestion for mass
772 spectrometric characterization of proteins and proteomes. *Nat Protoc* **1**: 2856-60
773 47. Rappsilber J, Ishihama Y, Mann M (2003) Stop and go extraction tips for matrix-
774 assisted laser desorption/ionization, nanoelectrospray, and LC/MS sample pretreatment in
775 proteomics. *Anal Chem* **75**: 663-70
776 48. Michalski A, Damoc E, Hauschild JP, Lange O, Wieghaus A, Makarov A, Nagaraj N, Cox
777 J, Mann M, Horning S (2011) Mass spectrometry-based proteomics using Q Exactive, a high-
778 performance benchtop quadrupole Orbitrap mass spectrometer. *Mol Cell Proteomics* **10**:
779 M111 011015
780 49. Cox J, Mann M (2008) MaxQuant enables high peptide identification rates,
781 individualized p.p.b.-range mass accuracies and proteome-wide protein quantification. *Nat*
782 *Biotechnol* **26**: 1367-72

783 50. Cox J, Neuhauser N, Michalski A, Scheltema RA, Olsen JV, Mann M (2011)
784 Andromeda: a peptide search engine integrated into the MaxQuant environment. *J*
785 *Proteome Res* **10**: 1794-805
786 51. Cox J, Hein MY, Luber CA, Paron I, Nagaraj N, Mann M (2014) Accurate proteome-
787 wide label-free quantification by delayed normalization and maximal peptide ratio
788 extraction, termed MaxLFQ. *Mol Cell Proteomics* **13**: 2513-26
789 52. Tyanova S, Temu T, Sinitcyn P, Carlson A, Hein MY, Geiger T, Mann M, Cox J (2016)
790 The Perseus computational platform for comprehensive analysis of (prote)omics data. *Nat*
791 *Methods* **13**: 731-40
792 53. Sato T, Stange DE, Ferrante M, Vries RG, Van Es JH, Van den Brink S, Van Houdt WJ,
793 Pronk A, Van Gorp J, Siersema PD*, et al.* (2011) Long-term expansion of epithelial organoids
794 from human colon, adenoma, adenocarcinoma, and Barrett's epithelium. *Gastroenterology*
795 **141**: 1762-72
796 54. Koo BK, Stange DE, Sato T, Karthaus W, Farin HF, Huch M, van Es JH, Clevers H (2011)
797 Controlled gene expression in primary Lgr5 organoid cultures. *Nat Methods* **9**: 81-3
798
799

800 **Figure legends**

Figure 1

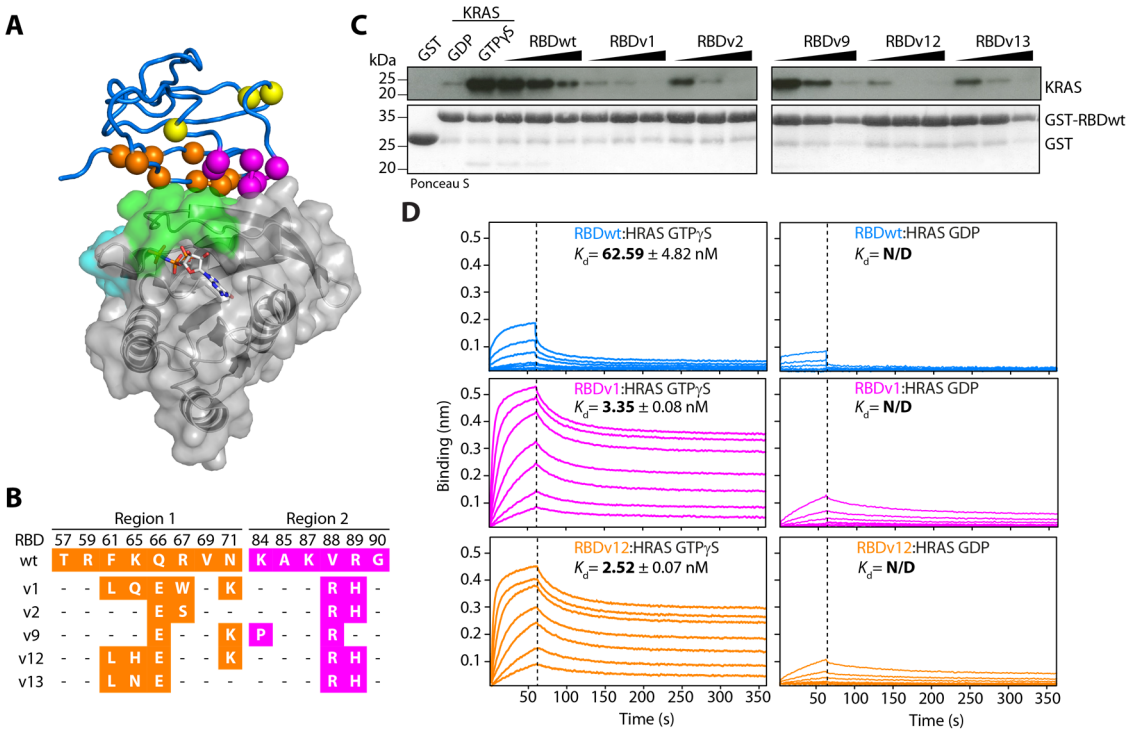

801

802

803 **Figure 1 - CRAF-Ras-binding domain (RBD) library design and selected RBD variants (RBDvs)**
804 **outcompete RBDwt by binding with highly improved affinity to active Ras.**

805 (**A**) CRAF-RBD in complex with HRAS (pdb: 4G0N) [5]. The RBD is shown as blue tube and
806 HRAS as transparent surface representation indicating the location of switch 1 (green) and
807 switch 2 (cyan). Residues modified in region 1 (orange), region 2 (magenta) and Cys to Ser
808 mutations (yellow) of CRAF-RBD are shown as colored spheres.

809 (**B**) Sequences of RBDvs selected by phage display. Residues in region 1 and region 2 are
810 colored as in (A). Non-mutated positions are indicated by dashes.

811 (**C**) *In vitro* competition of His-tagged GTPγS-loaded KRAS binding to GST-tagged RBDwt
812 immobilized on glutathione sepharose resin with increasing molar ratios of His-tagged RBDvs
813 or RBDwt (1:1, 1:2.5 and 1:10). KRAS bound to beads was detected by immunoblot and the
814 corresponding Ponceau S stained membrane is shown.

815 (**D**) Binding of GTPγS- and GDP-loaded HRAS to immobilized GST-tagged RBDwt (blue),
816 RBDv1 (magenta) or RBDv12 (orange) measured by bio-layer interferometry (BLI).
817 Concentrations of Ras ranged from 1 µM to 15.6 nM in a 1:1 dilution series. K_d values for
818 each experiment are shown.

Figure 2

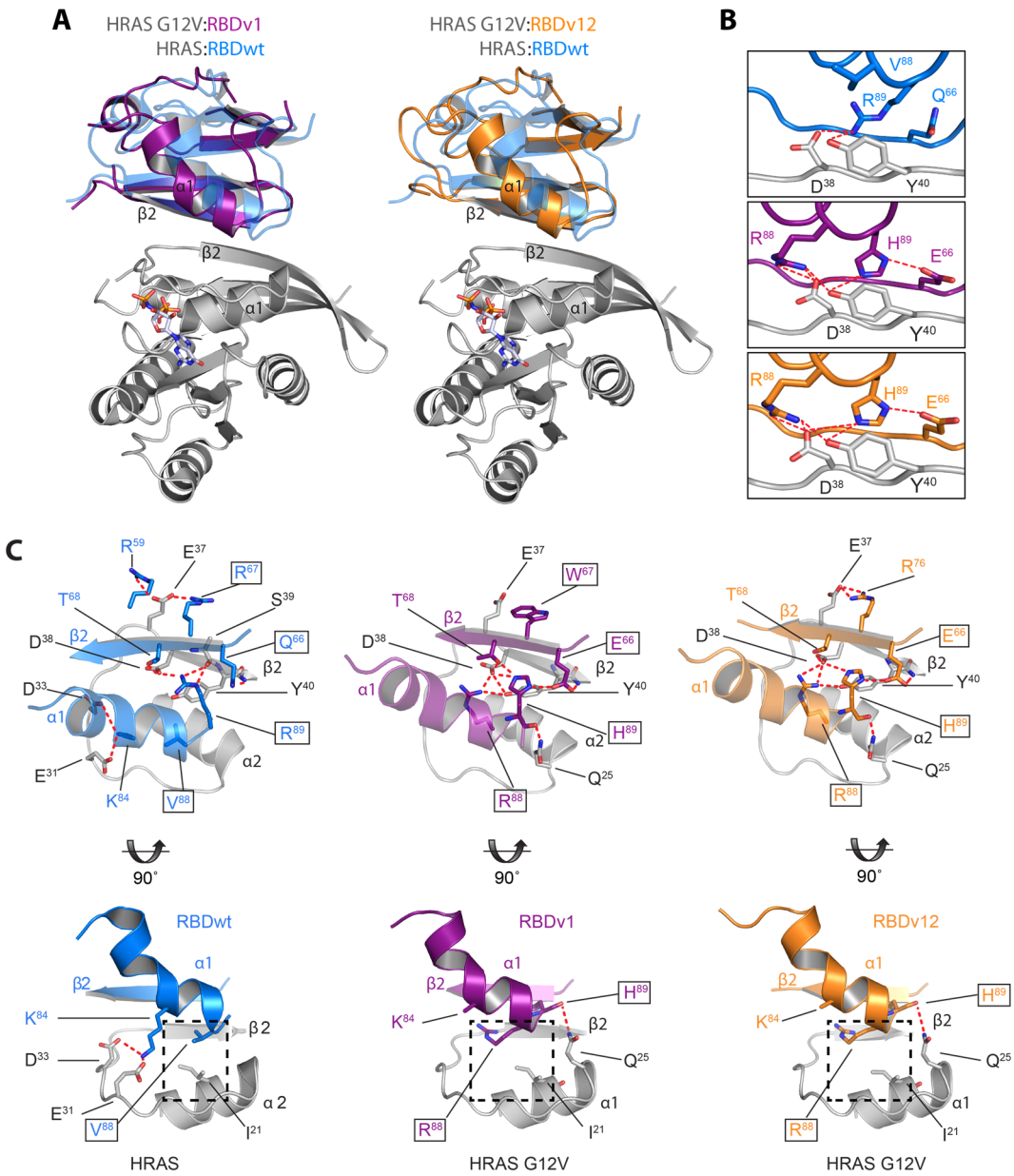

Figure 2 - RBDvs bind at the Ras effector binding site.

(**A**) Crystal structures of HRAS G12V (grey) in complex with RBDv1 (magenta) at 2.9 Å or RBDv12 (orange) at 3.15 Å resolution. Both structures are superimposed on HRAS in complex with RBDwt (blue) (pdb: 4G0N) [5]. For clarity, only HRAS G12V and the GTP analog phosphoaminophosphonic acid-guanylate ester (GNP) is shown as colored sticks.

(**B**) Side by side comparison of HRAS in complex with RBDwt (upper panel), RBDv1 (middle panel) or RBDv12 (lower panel) showing changes caused by mutations at positions 66, 88 and 89. Polar interactions are indicated by dashed lines (red). HRAS G12V, RBDwt, RBDv1

829 and v12 main and side chains are colored as in (A). Residues are numbered according to the
830 PDB entry for 4G0N.
831 (**C**) Top and side view of the binding interface of RBDwt and RBDvs with HRAS. Residues
832 involved in intermolecular interactions are shown as stick. Residues that are mutated in
833 RBDvs are highlighted by a black square. 90° rotated side view highlights the steric clash
834 between Ile^{21} in HRAS and Val^{88} to Arg in RBDvs that is involved in a shift of the α1-helix of
835 the RBDvs relative to that observed in RBDwt.
836

Figure 3

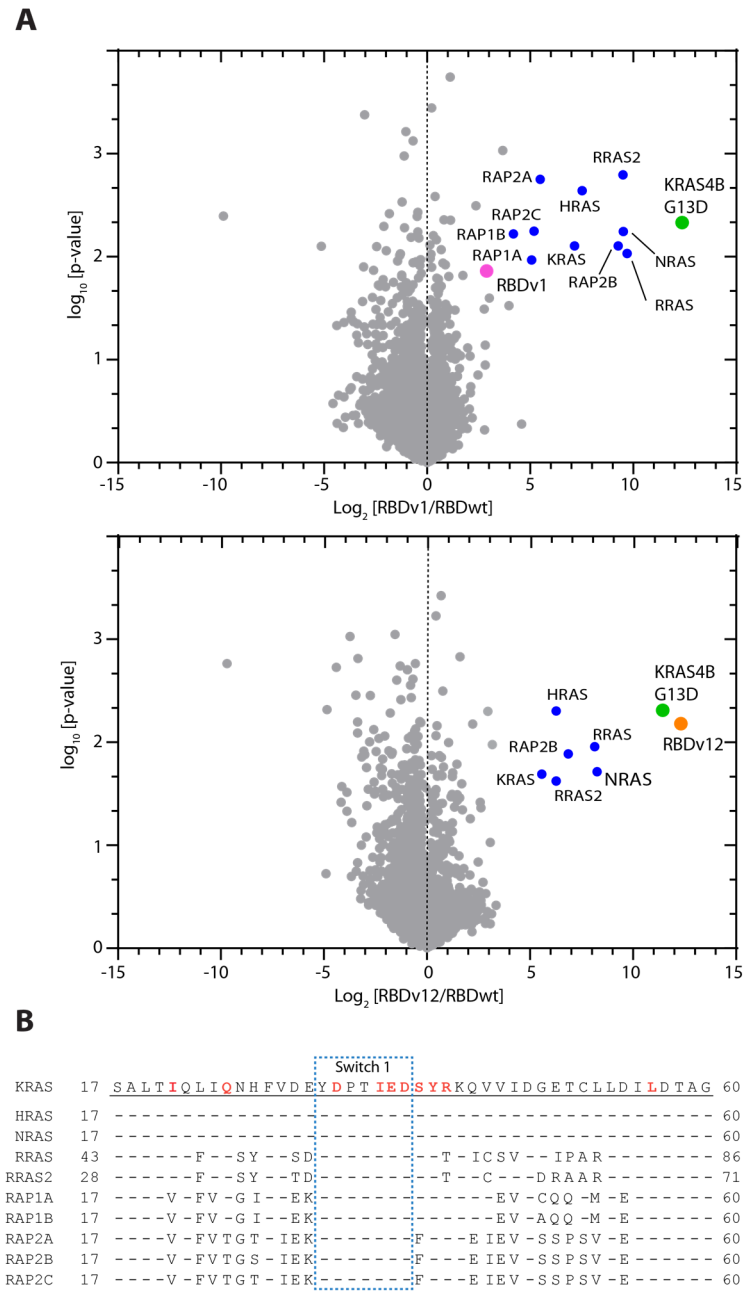

Figure 3 - RBDvs are specifically binding to endogenous KRAS4B G13D in HCT 116 cells. (**A**) Mass spectrometry of co-immunoprecipitation using anti-HA beads from lentiviral transduced HCT 116 cells stably expressing HA-tagged RBDwt, RBDv1 and RBDv12 upon induction with doxycycline (DOX) (1 µg/ml, 24h). Detected proteins (grey) were plotted as $\log_2$ average protein intensity for RBDv1/RBDwt (upper panel) or RBDv12/RBDwt (lower panel) versus $\log_{10}$ p-value. Only proteins that have been identified with a p-value < 0.05 are

845 shown (n=2). More than 16-fold enriched proteins and the RBDvs are shown as indicated
846 (colored symbols).
847 (**B**) Sequence alignment of Ras GTPases that have been enriched more than 16-fold (log_2 >
848 4). Conserved residues relative to KRAS are indicated as dashes. Switch 1 residues (blue box)
849 and residues within 4.5 Å of RBDvs (magenta) are highlighted.
850

Figure 4

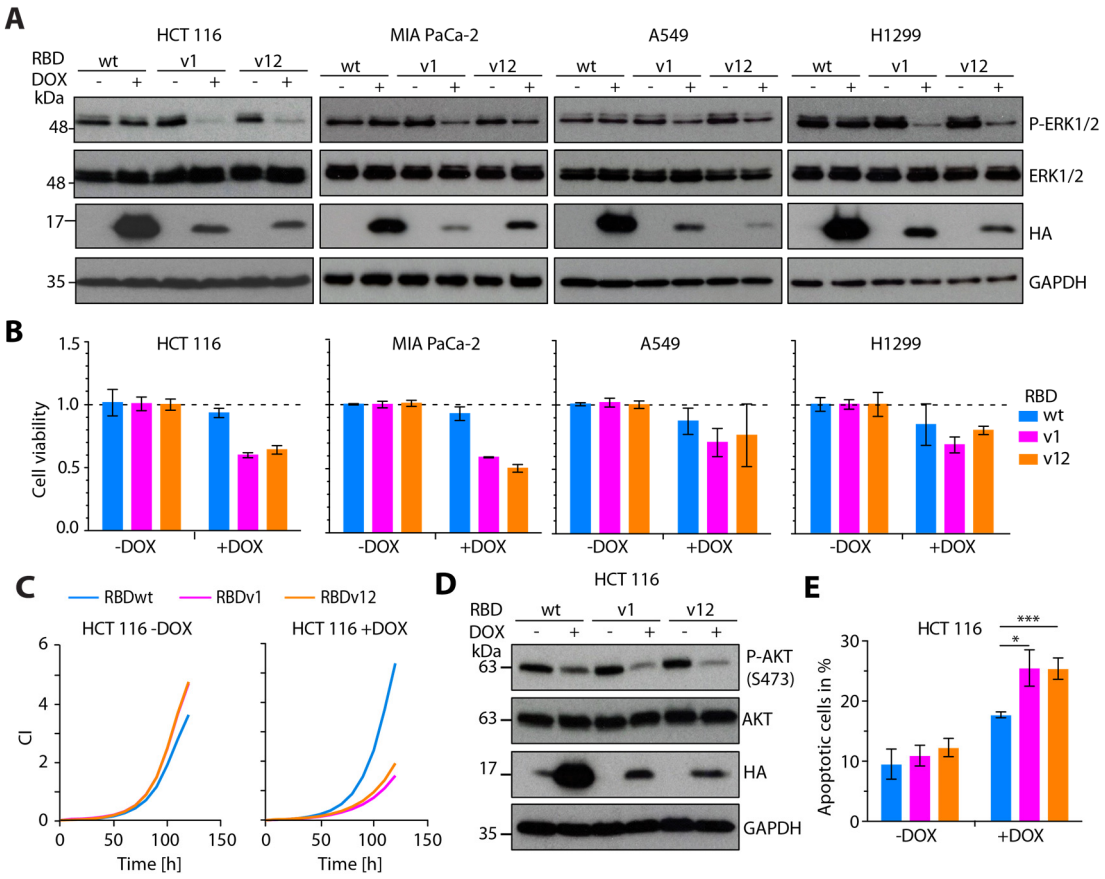

Figure 4 - RBDvs inhibit MAPK and PI3K signaling in cancer cells, reduce cellular viability and induce apoptosis in HCT 116 cells.

(**A**) Immunoblot of whole cell lysates from HCT 116, MIA PaCa-2, A549 and H1299 stably transduced with inducible lentiviral constructs expressing HA-tagged RBDwt, RBDv1 or RBDv12 in absence (-) and presence (+) of DOX (1 µg/ml, 24 h). Cell lysates were analyzed using the indicated antibodies.

(**B**) Normalized cell viability from cells used in panel (A) transduced with RBDwt (blue), RBDv1 (magenta) or RBDv12 (orange) measured as cellular ATP content by luciferase mediated bioluminescence. Reduction of cellular ATP in presence of RBDs (+DOX) was monitored after 120 h induction and normalized to the luminescence of non-induced control (-DOX) cells. (Error bars corresponds to ± standard deviation (SD) of 3 biological replicates (n=3).

(**C**) Cellular growth measured following cell index (CI) over time (h) by Real-time cell analysis (RTCA) of HCT 116 cells in absence or presence of DOX (1 µg/ml, 120 h). The mean of two technical replicates is shown.

868 (**D**) Immunoblot of whole cell lysates from HCT 116 stably transduced with RBDwt, RBDv1 or
869 RBDv12 in absence (-) and presence (+) of DOX (1 µg/ml, 24 h). Cell lysates were analyzed
870 using the indicated antibodies.
871 (**E**) Quantification of flow cytometry data of annexin V antibody and propidium iodide (PI)
872 stained HCT 116 cells cultured under full medium conditions in absence (-DOX) or presence
873 (+DOX) (1 µg/ml, 72 h). (Error bars corresponds to ± standard deviation (SD) of 3 biological
874 replicates (n=3). P-values were calculated by an unpaired t test ($^{*}P< 0.05$, *P< 0.01, $^{***}P<$
875 0.005).
876

Figure 5

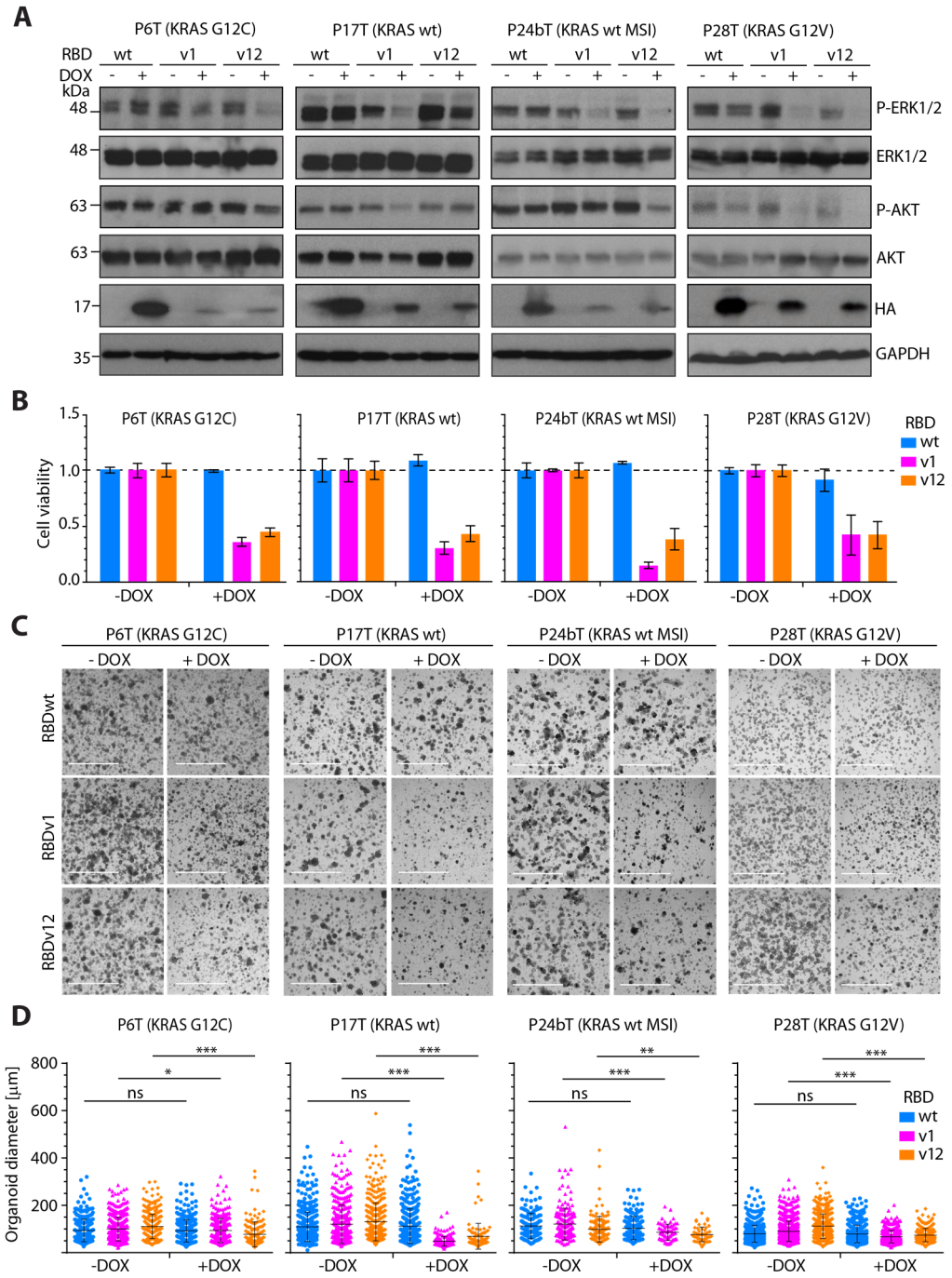

Figure 5 - Patient-derived colorectal cancer (CRC) organoids show reduced MAPK and AKT signaling and reduced cell viability upon RBDvs expression.

(**A**) Immunoblot of whole cell lysates derived from indicated patient-derived CRC organoids stably transduced with lentivirus encoding HA-tagged RBDwt, RBDv1 and RBDv12 in absence (-) or presence (+) of DOX (2 µg/ml, 72 h). Cell lysates were analyzed using indicated antibodies.

885 (**B**) Cellular ATP content of organoid cultures used in (A) expressing RBDwt (blue), RBDv1
886 (magenta) and RBDv12 (orange) was measured in a luciferase mediated bioluminescence
887 assay. Reduction of cellular ATP in presence of RBDvs (+DOX) in P17T and P24bT was
888 monitored after 72 h induction and normalized to the luminescence of non-induced control
889 organoids (-DOX) (2 µg/ml, 72 h). P6T and P28T stable organoids were seeded as single cells
890 and induced for 96 h and analyzed as above. Error bars correspond to ± SD of three technical
891 replicates (n=3).
892 (**C**) Bright field microscope images of organoid cultures used in (A) in presence (+) or absence
893 (-) of DOX (2 µg/ml, 72 h). Scale bars correspond to 2 mm. P=patient; T=tumor,
894 MSI=microsatellite instability.
895 (**D**) Quantification of organoid size in presence and absence of DOX (2 µg/ml, 2-6 d) from
896 bright field microscope images of organoid lines used in (A).
897 Error bars correspond to ± SD. Statistics were calculated using the Mann-Whitney U-test ($^{*}P<$
898 0.05, $^{**}P<0.01$ and $^{***}P<0.005$).
899

900

901

Table 1: Summary of response to Ras inhibition and mutational status of tested CRC organoids

HUB tumor organoid[29]	Organoid response in presence of RBDvs				Published mutational status[29]				
	pERK	pAKT	Cell Viability	Colony growth	Geftinib sensitivity	KRAS	NRAS	BRAF	PI3K
P6T	↓	–	↓	↓	resistant	G12C	wt	wt	wt
P26T	–	–	–	–	resistant	G12V	wt	wt	wt
P28T	↓	↓	↓	↓	sensitive	G12V	wt	wt	wt
P17T	↓	↓	↓	↓	sensitive	wt	wt	wt	wt
P18T	–	–	–	–	resistant	wt	wt	wt	wt
P20T	–	–	–	–	sensitive	wt	wt	wt	wt
P24bT (MSI)	↓	↓	↓	↓	n/a	wt	wt	wt	wt

P: patient; T: tumor; MSI: Microsatellite instability

902
903